JCI insight

ROR1-CAR T-cells are effective against lung and breast cancer in advanced microphysiologic 3D tumor models

Lars Wallstabe, … , Sarah L. Nietzer, Michael Hudecek

JCI Insight. 2019. https://doi.org/10.1172/jci.insight.126345.

Technical Advance In-Press Preview **Immunology** **Oncology**

Solid tumors impose immunological and physical barriers to the efficacy of chimeric antigen receptor (CAR) T-cell therapy that are not reflected in conventional pre-clinical testing against singularized tumor cells in two-dimensional culture. Here, we established microphysiologic three-dimensional (3D) lung and breast cancer models that resemble architectural and phenotypical features of primary tumors, and evaluated the anti-tumor function of ROR1-specific CAR T-cells. 3D tumors were established from A549 (non-small cell lung cancer) and MDA-MB-231 (triple-negative breast cancer) cell lines on a biological scaffold with intact basement membrane (BM) under static and dynamic culture conditions, which resulted in progressively increasing cell mass and invasive growth phenotype (dynamic>static; MDA-MB-231>A549). Treatment with ROR1-CAR T-cells conferred potent anti-tumor effects. In dynamic culture, CAR T-cells actively entered arterial medium flow, adhered to and infiltrated the tumor mass. ROR1-CAR T-cells penetrated deep into tumor tissue and eliminated multiple layers of tumor cells located above and below the BM. The microphysiologic 3D tumor models developed in this study are standardized scalable test systems that can be used either in conjunction with or in lieu of animal testing to interrogate the anti-tumor function of CAR T-cells, and to obtain proof-of-concept for their safety and efficacy prior to clinical application.

Title

ROR1-CAR T-cells are effective against lung and breast cancer in advanced microphysiologic 3D tumor models

Authors and affiliations

Lars Wallstabe[1,*], Claudia Göttlich[2,3,*], Lena C. Nelke[2,*], Johanna Kühnemundt[2,*], Thomas Schwarz[2,3], Thomas Nerreter[1], Hermann Einsele[1], Heike Walles[2,3], Gudrun Dandekar[2,3,**], Sarah L. Nietzer[2,§,**] and Michael Hudecek[1,§,**]

[1]Universitätsklinikum Würzburg, Medizinische Klinik und Poliklinik II, Oberdürrbacherstrasse 6, 97080 Würzburg, Germany

[2]Universitätsklinikum Würzburg, Tissue Engineering and Regenerative Medicine, Röntgenring 11, 97070 Würzburg, Germany

[3]Fraunhofer Institute for Silicate Research, Translational Center Regenerative Therapies, Röntgenring 11, 97070 Würzburg, Germany

* L. Wallstabe, C. Göttlich, L.C. Nelke & J. Kühnemundt contributed equally to this work.

** S.L. Nietzer, G. Dandekar & M. Hudecek contributed equally to this work.

[§]Corresponding authors

Corresponding authors

for CAR T-cells: Michael Hudecek, MD, Universitätsklinikum Würzburg, Medizinische Klinik und Poliklinik II, Oberdürrbacherstrasse 6, 97080 Würzburg, GER, phone: +4993120171092, Email: hudecek_m@ukw.de

for 3D models: Sarah L. Nietzer, PhD, Universitätsklinikum Würzburg, Tissue Engineering and Regenerative Medicine, Röntgenring 11, 97070 Würzburg, GER, phone: +499313182596 Email: sarah.nietzer@uni-wuerzburg.de

Conflicts of interest

M.H. is inventor on patents related to CAR technologies that have been filed by the Fred Hutchinson Cancer Research Center (Seattle, WA) and licensed by JUNO Therapeutics Inc., and that have been filed by the Julius Maximilians University Würzburg (Würzburg, Germany).

Abstract

Solid tumors impose immunological and physical barriers to the efficacy of chimeric antigen receptor (CAR) T-cell therapy that are not reflected in conventional pre-clinical testing against singularized tumor cells in two-dimensional culture. Here, we established microphysiologic three-dimensional (3D) lung and breast cancer models that resemble architectural and phenotypical features of primary tumors, and evaluated the anti-tumor function of ROR1-specific CAR T-cells. 3D tumors were established from A549 (non-small cell lung cancer) and MDA-MB-231 (triple-negative breast cancer) cell lines on a biological scaffold with intact basement membrane (BM) under static and dynamic culture conditions, which resulted in progressively increasing cell mass and invasive growth phenotype (dynamic>static; MDA-MB-231>A549). Treatment with ROR1-CAR T-cells conferred potent anti-tumor effects. In dynamic culture, CAR T-cells actively entered arterial medium flow, adhered to and infiltrated the tumor mass. ROR1-CAR T-cells penetrated deep into tumor tissue and eliminated multiple layers of tumor cells located above and below the BM. The microphysiologic 3D tumor models developed in this study are standardized scalable test systems that can be used either in conjunction with or in lieu of animal testing to interrogate the anti-tumor function of CAR T-cells, and to obtain proof-of-concept for their safety and efficacy prior to clinical application.

Introduction

Adoptive immunotherapy with gene-engineered chimeric antigen receptor (CAR) T-cells has obtained clinical proof-of-concept in hematologic cancers with CD19 as exemplary target antigen in B-cell leukemia and lymphoma (1–3). A current focus in the field is to expand applications of CAR T-cell therapy from relatively rare hematologic malignancies to prevalent solid tumors. We are pursuing the receptor tyrosine kinase-like orphan receptor 1 (ROR1) as target antigen for CAR T-cells in several hematologic malignancies and solid tumors (4, 5). Uniform high level expression of ROR1 protein was first shown in B-cell chronic lymphocytic leukemia, mantle cell lymphoma and a subset of acute lymphoblastic leukemia and recently also in distinct histologic subsets of prevalent epithelial cancers including lung, breast, colon, pancreas, renal and ovarian cancers (6–8). We have demonstrated in previous work that ROR1 has only very limited expression in normal adult tissues and performed toxicology studies in non-human primates that did not reveal toxicity of ROR1-directed immunotherapy to vital normal organs (9). In addition, there is evidence for a critical role of ROR1 in malignant transformation and oncogenic signaling that support the use of ROR1 as a target in cancer immunotherapy (10).

We have recently reported on the development of a ROR1-specific CAR with optimized targeting domain affinity and extracellular spacer design that confers specific recognition and potent reactivity against ROR1$^+$ lymphoma in pre-clinical models in vitro and in vivo (5, 11). We have also demonstrated that CD8$^+$ T-cells expressing this ROR1-CAR are capable of conferring cytolysis of MDA-MB-231 triple-negative breast cancer (TNBC) cells in conventional 2D co-culture (5). While encouraging, the use of singularized tumor cells in 2D culture is simplistic and does not consider the specific challenges in tumor architecture, phenotype and microenvironment that CAR T-cells encounter when combating a solid tumor. In the present study we are therefore evaluating the anti-tumor function of ROR1-CAR T-cells in microphysiologic 3D tumor models that reflect these challenges more realistically and provide an alternative to testing in animal models.

We have in previous work established protocols for the engineering of vascularized and non-vascularized 3D tissues in bioreactors (BioVaSc-TERM® technology) (12). The BioVaSc is derived from decellularized porcine jejunum and used as a collagen scaffold with intact basement membrane (BM) that permits the engraftment and propagation of normal and cancerous (OncoVaSc-TERM®) epithelial tissues in 3D culture. We have recently demonstrated the development of a 3D lung tumor from A549 non-small cell lung cancer (NSCLC) using the BioVaSc technology (13–15). The A549 tumor model employs the non-vascular part of the BioVaSc - the small intestinal submucosa and mucosa (SISmuc) - for cell engraftment. Intriguingly, the resulting lung tumor resembled the architecture of primary lung carcinomas, and recapitulated ‘real-life’ pathophysiologic features including growth kinetic, tumor cell migration and invasion, and epithelial-to-mesenchymal transition after stimulation with TGF-β1 (13, 14).

Here we established microphysiologic 3D tumor models of A549 NSCLC and MDA-MB-231 TNBC using the SISmuc technology to assess the anti-tumor function of ROR1-CAR T-cells. We obtained 3D tumors with considerable cell mass and demonstrate that ROR1-CAR T-cells rapidly infiltrate and migrate through the 3D tumor tissue, and confer a specific and potent anti-tumor effect over a several day time course. ROR1-CAR T-cells were able to sustain their cytolytic activity, cytokine secretion and proliferation for several days in culture but displayed functional and phenotypic indicators of T-cell exhaustion at the end of the analysis period. The data illustrate the utility of microphysiologic 3D culture systems for evaluating CAR T-cell performance beyond the scope of conventional testing in 2D in vitro and xenograft animal models.

Results

Invasive growth of A549 lung and MDA-MB-231 breast cancer in 3D culture

We established microphysiologic 3D models of NSCLC (A549 cell line) and TNBC (MDA-MB-231 cell line) using the SISmuc platform. First, we applied static culture conditions in cell crowns (i.e. two metal rings for matrix fixation) and performed histopathologic analysis on cross-sections of the resulting tumors after 14 days of incubation (Figure 1, Supplemental Figure 1A). Staining was performed for the epithelial marker pan-cytokeratin (PCK) to detect tumor cells and collagen IV (Col IV) to detect extracellular matrix (ECM). Tumor architecture was evaluated using a customized grading system (Table 1). We found that A549 tumor cells formed a confluent monolayer that populated the entire SISmuc area and settled deep into crypts. However, A549 cells did not cross the basement membrane (Grade 1) (Figure 1). The distribution of MDA-MB-231 cells was more scattered on the SISmuc surface, and denser within crypts. Remarkably, there were MDA-MB-231 cells that had crossed the basement membrane barrier and had migrated into the matrix of the former mucosa compartment (Grade 2) (Figure 1). For each cell line, this architecture and phenotype was confirmed in >10 replicate experiments that we established on distinct batches of SISmuc scaffold.

In the next set of experiments, we applied dynamic culture conditions in a flow bioreactor to establish a larger tumor mass of A549 and MDA-MB-231 cells on our SISmuc platform. Histopathologic analysis was performed on day 14 after transfer to the bioreactor (Figure 1; Supplemental Figure 1B). We found that the mass of A549 cells had considerably increased compared to the static culture model and comprised several layers of tumor cells that spanned the entire scaffold surface. In addition, there was a higher degree of migration with A549 cells packing the entire lumen of crypt structures, and invasion of A549 cells across the basement membrane (Grade 2) (Figure 1). Also with MDA-MB-231 cells, there was a substantial increase in tumor mass in the dynamic compared to the static culture system, and a shift to an aggressive and destructive growth phenotype. The data show that MDA-MB-231 cells had infiltrated the entire SISmuc matrix and crossed the barrier between former mucosa and submucosa compartment (Grade 3). Accordingly, the MDA-MB-231 tumors displayed high-level expression of the mesenchymal marker vimentin (Vim), consistent with epithelial-mesenchymal transition (Figure 1). This architecture and phenotype was obtained consistently in >10 independent experiments with distinct batches of SISmuc scaffold. We confirmed that A549 and MDA-MB-231 cells that we isolated from the 3D tumors had retained uniform expression of the ROR1 antigen (Supplemental Figure 2).

Taken together, these data show that microphysiologic 3D tumor models of breast and lung cancer can be established on the SISmuc platform using the A549 and MDA-MB-231 cell lines. The use of static and dynamic culture conditions, respectively, provides tumors with increasing cell mass and distinct architectural features that permit interrogating the anti-tumor function of CAR T-cells in an increasingly challenging microenvironment.

ROR1-CAR T-cells eliminate large 3D masses of lung and breast cancer

We sought to determine whether ROR1-specific CAR T-cells are able to mediate an anti-tumor effect in the 3D A549 lung and MDA-MB-231 breast cancer models under static conditions (Grade 1 & 2, respectively). In this set of experiments, we used an optimized ROR1-CAR comprising a targeting domain specific for the R12 epitope, a short IgG4-Fc hinge spacer, and a 4-1BB_CD3ζ signaling module (5). We treated tumors with increasing concentrations of $CD8^+$ ROR1-CAR modified or non-CAR-modified control T-cells (Figure 2A) (dose range: $5x10^4$ – $1x10^6$) and performed M30-ELISA to detect caspase-cleaved keratin 18 as a measure for tumor cell apoptosis over a 3-day period. Experiments were done in n=4 biological replicates with T-cell lines from different donors. Indeed, we found that ROR1-CAR T-cells conferred a specific and potent anti-tumor effect in the 3D models. There was a higher M30-ELISA signal at each analysis time point (starting at 24 h) and in each of the A549 and MDA-MB-231 cell crowns that we had treated with ROR1-CAR T-cells compared to control T-cells (Figure 2B). The anti-tumor effect was dose-dependent, e.g. with higher doses of CAR T-cells, there was a higher peak ELISA signal and the peak signal occurred earlier during the 3-day analysis period. When we administered $5x10^5$ or $1x10^6$ ROR1-CAR T-cells to A549 lung cancer, the peak ELISA signal was obtained during the 6-24 h time interval, with an 11.2-fold and 14.5-fold increase in apoptosis-induction compared to control T-cells, respectively (Figure 2B). When we administered $2.5x10^5$ ROR1-CAR T-cells to A549 lung cancer, the peak ELISA signal was obtained during the 24-48 h interval, and at doses < $2.5x10^5$ ROR1-CAR T-cells, the peak signal was obtained during the 48-72 h interval (Figure 2B). Of note, the M30-ELISA specifically measures apoptosis of cells with epithelial phenotype and accordingly, we obtained a higher overall signal in the A549 lung cancer model compared to the MDA-MB-231 breast cancer model, as the latter cell line has a partly mesenchymal phenotype (Figure 1).

We obtained medium samples at 6 h, 24 h, 48 h and 72 h during the 3-day incubation period and detected high levels of IFN-γ at each analysis time point after treatment with ROR1-CAR T-cells. The amount of IL-2 that we detected by ELISA declined between the 24 h and 72 h time point, indicating that IL-2 had been consumed by activated CAR T-cells (Figure 2C). The magnitude of IFN-γ and IL-2 release by ROR1-CAR T-cells was similar in the A549 and the MDA-MB-231 models. Flow cytometric analysis on T-cells on day 3 showed uniform expression of the activation markers CD25 and CD69 on ROR1-CAR T-cells, but not on non-CAR modified control T-cells (Figure 2D). Together, these data show that ROR1-CAR T-cells mediate a specific anti-tumor effect against 3D microphysiologic tumor models of A549 lung cancer and MDA-MB-231 breast cancer under static culture conditions.

ROR1-CAR T-cells sustain their anti-tumor function for several days in 3D culture

We extracted the SISmuc scaffolds on day 3 after T-cell administration and prepared cross-sections for immunofluorescent staining. We performed co-staining for CD45 and DAPI to distinguish T-cells ($CD45^+DAPI^+$) and tumor cells ($CD45^-DAPI^+$). These analyses confirmed that ROR1-CAR T-cells had

induced a specific and very potent anti-tumor effect against A549 NSCLC and MDA-MB-231 TNBC models. In particular, the data show that ROR1-CAR T-cells had attached to the apical tumor cell layer, migrated through the basement membrane and SISmuc matrix and could be detected in the former mucosa compartment (Figure 3A). On high-power resolution, the direct interaction of ROR1-CAR T-cells with A549 and MDA-MB-231 tumor cells could be visualized (Figure 3B). Overall, the number of infiltrating T-cells in the scaffold correlated with the number of T-cells that had been administered (Figure 3A). Even at the lowest CAR T-cell dose level, a substantial proportion of tumor cells had been eliminated, regardless of how deeply tumor cells had migrated into crypts and the tissue matrix. Co-staining for CD45 and Ki67 and cell counting confirmed that there was an increase in absolute ROR1-CAR T-cell number on day 3 after administration and a high rate of productive proliferation in ROR1-CAR T-cells (Figure 3C).

In summary, these data show that ROR1-CAR T-cells are able to infiltrate and migrate through the tumor matrix and maintain their function for at least 72 h after administration under static culture conditions. ROR1-CAR T-cells were capable of eliminating tumor cells that were harbored in crypt structures and ECM on the contralateral side of the basement membrane, indicating they possess and maintain a substantial migratory capacity within the tumor mass.

PD-1 induction on CAR T-cells after exposure to tumor cells in 3D culture

We analyzed expression of PD-1 on ROR1-CAR modified and non-CAR modified control T-cells at the end of the assay period in the static A549 lung cancer and MDA-MB-231 breast cancer models. We detected PD-1 on both, $CD8^+$ and $CD4^+$ ROR1-CAR T-cells (CD4 > CD8) (Supplemental Figure 3A+B). There were higher levels of PD-1 on ROR1-CAR T-cells that had been exposed to MDA-MB-231 breast cancer cells compared to A549 lung cancer cells (Supplemental Figure 3A+B). ROR1-CAR T-cells that we had maintained in assay medium without exposure to tumor cells served as reference. No significant difference in PD-1 expression was detected between control T-cells that had been exposed to tumor cells or maintained in assay medium. Of note, we detected uniform expression of PD-L1 on MDA-MB-231 cells and A549 cells (MDA-MB-231 > A549) (Supplemental Figure 3C). These data confirm that ROR1-CAR T-cells undergo specific activation in 3D culture and suggest that, depending on the particular tumor model, CAR T-cells may enter differential grades of activation and exhaustion.

Variations in CAR targeting domain and spacer design affect anti-tumor function in 3D culture

We were interested in determining whether testing in 3D culture can disclose differences in anti-tumor function between ROR1-CAR constructs that comprise distinct targeting domains and spacer designs. We used the ROR1-CAR with ‘high affinity’ R12 targeting domain, customized short IgG4-Fc hinge spacer and 4-1BB_CD3ζ signaling module, that we had previously ‘optimized’ in 2D in vitro culture

and xenograft in vivo models as reference and used a 'suboptimal' ROR1-CAR with 'low affinity' 2A2 targeting domain for comparison (5). In this set of experiments, we employed the A549 lung cancer model under static culture conditions. First, we showed that also the 2A2 ROR1-CAR worked best with a short IgG4-Fc hinge spacer rather than a long IgG4-Fc hinge-C_H2-C_H3 spacer domain, as demonstrated by superior production of IFN-γ and IL-2 in 3D culture (Supplemental Figure 4). This confirmed our prior data in conventional 2D in vitro culture that had identified the short spacer as the optimal configuration for targeting the 2A2 ROR1 epitope (5). Then, we compared the anti-tumor function of T-cells expressing the R12 and 2A2 ROR1-CAR constructs in 3D culture. We found stronger apoptosis induction with the R12 ROR1-CAR, most evident when ROR1-CAR T-cells were administered at a low dose ($5x10^4$). At this dose, the peak signal in the M30-ELISA was obtained in the 24-48h interval. When ROR1-CAR T-cells were administered at higher doses ($2.5x10^5$ – $1x10^6$), the M30-ELISA signal obtained with the two ROR1-CAR constructs was similar. At the $1x10^6$ dose level, the peak M30-ELISA signal was already obtained in the 6-24h interval (Figure 4A). The R12 ROR1-CAR induced stronger IFN-γ and IL-2 production compared to the 2A2 ROR1-CAR at each of the analysis time points. Peak IFN-γ production occurred in the 6-24h interval, and peak IL-2 production occurred in the first 6h of the assay period (Figure 4B). By flow cytometric analysis, we detected uniform expression of the activation markers CD25 and CD69 on R12 ROR1-CAR T-cells and 2A2 ROR1-CAR T-cells at the end of the 72-hour assay period (Figure 4C). From this comparison, the R12 ROR1-CAR emerged as the superior construct and was therefore advanced to further evaluation in dynamic 3D culture.

Taken together, these data show that ROR1-CAR constructs that differ in targeting domain and spacer design confer different degrees of reactivity in 3D culture. These data affirm our prior notion that variations in CAR design affect tumor recognition and CAR T-cell function and suggest that test campaigns in 3D tumor models can be performed to identify CAR designs with optimal and suboptimal reactivity.

ROR1-CAR T-cells penetrate and destroy invasive 3D tumors in dynamic culture

Next, we assessed the performance of R12 ROR1-CAR T-cells against A549 lung cancer and MDA-MB-231 breast cancer in the dynamic culture system with constant medium flow in a closed circuit set-up (Grade 2 & 3, respectively). This set-up provides additional challenges because T-cells are administered into a medium reservoir and have to i) enter arterial medium flow, ii) adhere to and penetrate into the SISmuc tumor matrix, and iii) encounter a larger number of tumor cells compared to the static model. We treated tumors with a fixed dose of $10x10^6$ ROR1-CAR T-cells ($CD8^+$:$CD4^+$ at 1:1 ratio) (16) and performed M30-ELISA at 24 h intervals over a 5-day period. Experiments were done in n=4 biological replicates with T-cell lines from different donors. Again, we detected specific and very potent anti-tumor activity of ROR1-CAR T-cells against A549 lung cancer and MDA-MB-231 breast cancer (Figure 5A). With A549 lung cancer, apoptosis induction peaked between 24 h and 48 h after

ROR1-CAR T-cell transfer (7.7-fold higher compared to control T-cells) and continued over the entire 5-day period (Figure 5A). With MDA-MB-231 breast cancer, apoptosis induction peaked in the first 24 h after CAR T-cell administration (3.6-fold higher compared to control T-cells) and subsequently declined. Analysis of the culture medium by ELISA revealed that CAR T-cells had produced very high levels of IFN-γ and IL-2 (Figure 5B). At the end of the 5-day assay period, $CD8^+$ and $CD4^+$ ROR1-CAR T-cells displayed a highly activated phenotype as assessed by expression of CD25 and CD69 (Figure 5C, Supplemental Figure 5).

On day 5, we performed a detailed histopathologic analysis on the SISmuc scaffolds. We found that ROR1-CAR T-cells ($CD45^+DAPI^+$) had migrated throughout the entire tumor matrix (Figure 6A, white arrows) and were present at higher frequency compared to control T-cells. In the A549 lung cancer model, ROR1-CAR T-cells had eliminated multiple layers of tumor cells that had been located on top of the matrix, and significantly reduced the number of tumor cells in crypts. Non-CAR modified control T-cells did not convey a discernable anti-tumor effect. In the MDA-MB-231 breast cancer model, ROR1-CAR T-cells had removed a substantial proportion of tumor cells in the entire tissue matrix as evidenced by immune fluorescence staining for CD45/DAPI and PCK/ColIV (Figure 6A+B). In both tumor models, there was a high percentage of proliferating ROR1-CAR T-cells by Ki67 staining (Figure 6C), and a significant increase in absolute numbers of ROR1-CAR T-cells (Figure 6C).

Collectively, the data show that ROR1-specific CAR T-cells confer substantial anti-tumor reactivity against invasive A549 lung cancer and MDA-MB-231 breast cancer that have grown to comprise large cell masses and display a destructive phenotype. ROR1-CAR T-cells remain viable for several days in dynamic 3D culture and surmount physical and immunological barriers to exert their anti-tumor functions.

Discussion

The clinical proof-of-concept for the safety and efficacy of adoptive immunotherapy with CAR T-cells in prevalent solid tumors is still pending. The challenges that have been postulated for CAR T-cells to overcome include migrating through endothelial and stroma barriers surrounding the tumor cells, withstanding 'chronic' antigen exposure in a large tumor mass, and maintaining viability and function in the tumor microenvironment that is poised with immunosuppressive cytokines, cellular ligands and metabolites (17). Therefore, significant efforts are being invested in pre-clinical studies that seek to interrogate CAR T-cell anti-tumor function and to guide the evolution of CAR technologies beyond the point that is deemed necessary for achieving therapeutic efficacy in the clinical setting. A problem is that conventional pre-clinical test models do not reflect the unique attributes and challenges that are imposed by solid tumors. In the majority of pre-clinical studies, the potency of CAR T-cells is probed against singularized cells of established solid tumor cell lines in vitro at effector to target cell ratios that cannot be achieved in humans, and in murine xenograft models, where tumor cell lines are ectopically inoculated and form tumor lesions that do not resemble the architecture and phenotype of primary human tumors (18). Therefore, we set out to develop an alternative test system that incorporates physical and immunological barriers of solid tumors more realistically and focused on lung and breast cancer as the two most prevalent cancers in men and women.

The microphysiologic 3D tumor models employed in this study are based on a biological matrix derived from decellularized porcine jejunum that contains an intact BM and therefore permits rapid engraftment of epithelial cancer cells. We inoculated this matrix with two established and widely accepted tumor cell lines, A549 (NSCLC) and MDA-MB-231 (TNBC). Upon static and dynamic culture, tumors could be routinely established and displayed a consistent phenotype with characteristic architecture. There are several lines of evidence supporting the notion that the density and culture environment of immortalized tumor cell lines impacts their differentiation, signal transduction and drug sensitivity (19, 20). Indeed, we have shown in previous studies that tumor cells established on our 3D scaffold have a more realistic proliferation rate and differentiation state, drug sensitivity and response compared to tumor cells in conventional 2D culture (13, 15). In our dynamic 3D culture models with A549 cells and MDA-MB-231 cells, there were multiple layers of tumor cells and tumor cell aggregates in former crypts that provided a substantially greater challenge to CAR T-cells for conferring their anti-tumor reactivity compared to singularized tumor cells in 2D culture. We have shown in previous work with normal and malignant tissue models that the continuous medium flow in the dynamic 3D culture system results in superior nutrient supply and waste-product removal compared to the static culture system (21). Accordingly, the dynamic culture with constant medium flow yielded a greater tumor cell mass and supported the invasion of tumor cells beyond the basement membrane for both A549 lung cancer and MDA-MB-231 breast cancer in our microphysiologic 3D models. In particular, MDA-MB-231 cells displayed more rapid and more aggressive growth compared to A549 cells, consistent with previous studies in 2D in vitro and organoid culture that described the invasive potential of this cell line (22).

Several strategies for ex vivo testing of tumor-reactive T-cells have been proposed, including the use of suspension cultures or gel cultures with tumor organoids. Tumor organoids have been derived from A549 lung cancer and MDA-MB-231 breast cancer cells (23, 24). An advantage of organoids is that they are faster and easier to produce compared to microphysiologic 3D models and are easier to scale-up for high-throughput testing. However, organoids do not resemble primary tumor architecture and the tumor cell mass is much lower compared to our 3D models. Therefore, several critical features of CAR T-cells, including their ability to penetrate and migrate through tumor tissue and their response to chronic antigen exposure, cannot be adequately addressed in organoids. Another approach that has been proposed for evaluating the interaction of T-cells and solid tumor cells, is the use of a microscale fluidic device where tumor cells are inserted as single cells or cell aggregates in collagen gel and T-cells are supplemented in a parallel channel with directional medium flow (25). An advantage of this microfluidic model is that it is easier to obtain information on the performance of individual T-cells, even though the spatiotemporal resolution in this set-up is low. The microphysiologic 3D models described in our study are more laborious to establish compared to organoids and more difficult to set up compared to the microfluidic system. Importantly however, they can be scaled up to medium- and high-throughput testing and provide a global view on CAR T-cell performance. This view can even be refined by disassembling the 3D scaffold at the end of the assay to perform detailed histologic and phenotypic analyses on T-cells, as well as residual tumor and stroma cells.

The data obtained in our 3D lung and breast cancer models show that ROR1-CAR T-cells are able to penetrate and migrate through a tumor mass and confer a significant anti-tumor effect over a several day period. In the static 3D model, the adherence and migration of T-cells is supported by gravity. However, in the dynamic 3D model, ROR1-CAR T-cells had to actively adhere to and migrate into the tumor from the constant medium flow. The bioreactor used for dynamic culture is constructed as a single circuit that provides an even amount of pressure throughout the system. The SISmuc matrix is connected to the circuit on both the apical and the basal side, and therefore the same pressure applies on both sides. With these conditions, the bioreactor did not artificially favor ROR1-CAR T-cell migration into the tumor mass. We have determined that the shear stress exerted on T-cells in the bioreactor is 0.0004 dyn/cm^2 (21), which is below the physiological value measured in postcapillary venules of 3 - 30 dyn/cm^2 (26). By increasing the flow rate, shear stress can be enhanced to analyze its influence on T-cell adherence and migration into the tumor tissue in future studies.

We provide evidence that ROR1-CAR T-cells rapidly induced apoptosis of A549 and MDA-MB-231 tumor cells, produced high levels of cytokines and were induced to productively proliferate in both, the static and dynamic culture system displaying different grades of invasiveness. ROR1-CAR T-cells had a phenotype consistent with strong activation, i.e. they expressed high levels of CD25 and CD69. ROR1-CAR T-cells were also induced to express PD-1, which is commonly observed in activated but also in exhausted T-cells (27–29). Notably, we detected residual tumor cells at the end of the 3-day and 5-day time course in both, the static and dynamic culture system, and with both, the A549 lung cancer and the

MDA-MB-231 breast cancer models. Our histopathologic analyses did not reveal whether these residual tumor cells had still been alive or whether they had been in the process of apoptosis at the time of formalin fixation and paraffin embedding. However, we would speculate that these tumor cells had indeed been alive and had not been eliminated by ROR1-CAR T-cells during the assay period. This may indicate that the elimination of scattered residual tumor cells requires more time, or that ROR1-CAR T-cells were entering a state of exhaustion and were unable to eliminate these tumor cells. Accordingly, future study protocols in our 3D tumor models would consider administering a second dose of ROR1-CAR T-cells, or administering a combination treatment of ROR1-CAR T-cells and immune checkpoint inhibitors.

There is a continuous effort in the field to optimize existing and to develop novel CAR designs. We and others have shown in previous work that e.g. the choice of targeting domain, spacer design and signaling module affect tumor cell recognition and anti-tumor function of CAR T-cells (5, 11, 30). However, there is presently no consensus on whether a single or a combination of in vitro and in vivo assays constitute a 'gold standard' for evaluating CARs and for predicting safety and efficacy in humans (18). It seems plausible however to assume that conventional 2D (in vitro) test systems may be more useful for assessing 'short term' CAR T-cell effector functions such as e.g. cytolytic activity and cytokine secretion, whereas animal models (in vivo) may rather provide a 'long term' read-out of overall CAR T-cell performance including engraftment and proliferation. In this regard, the microphysiologic 3D models presented in this study are attractive because they provide information on both short and long term CAR T-cell functions. We have performed several test campaigns with ROR1-CAR T-cells in our 3D models and detected differences in anti-tumor function between CAR constructs with variable targeting domain, spacer domain and costimulatory domain that we had also noted in 2D test systems and in murine xenograft models in previous work (5). Of particular interest, we confirmed superior anti-tumor functions with ROR1-CAR T-cells expressing the 'high affinity' R12 targeting domain (0.11 nM) compared to the 'low affinity' 2A2 targeting domain (0.42 nM) (31, 32) in our 3D tumor models; higher cytokine secretion from T-cells expressing ROR1-CARs with CD28 compared to 4-1BB costimulatory domain (2A2 ROR1-CAR with CD28 costimulation, Supplemental Figure 4 vs. 2A2 ROR1-CAR with 4-1BB costimulation, Figure 4); and confirmed the previously 'optimized' R12 ROR1-CAR as the most potent construct, supporting its continuous pre-clinical and clinical development (9).

In the present study, we have focused on lung cancer and breast cancer to evaluate the anti-tumor function of ROR1-CAR T-cells. The SISmuc 3D culture system can be readily adapted to accommodate other cancer entities, as we have recently demonstrated for colorectal cancer (21, 33). The 3D tumor models employed in our study are based on a modular tissue engineering platform that can incorporate additional challenges for CAR T-cells. In previous work, we have demonstrated the potential to generate vascularized tissue from our BioVaSc scaffold by engrafting the ECM matrix of mesenteric artery and vein with human endothelial cells (34). Further, we have demonstrated the potential to include fibroblasts and other stroma cells into the extracellular SISmuc matrix, and are currently developing

protocols that allow including regulatory T-cells and myeloid-derived suppressor cells into our 3D culture system in order to better simulate the immunosuppressive tumor microenvironment.

The BioVaSc was originally designed for the generation of artificial normal human tissues in regenerative medicine. Several normal human tissues including trachea, myocardium, liver, skin, intestine and kidney have been generated on this platform (12, 35–40). Accordingly, we believe that there is a perspective not only for assessing efficacy in 3D tumor models, but also for assessing safety and tissue cross-reactivity of CAR T-cells in 3D normal tissue models. With our existing protocols, it is possible to generate approximately 130 SISmuc scaffolds from 1 porcine jejunum. Each scaffold can then be populated with different types of normal or malignant cells. The microphysiologic 3D models described in our study may therefore contribute to reducing the number of animals in rodent and non-human primate models that are involved in pre-clinical CAR T-cell research.

Methods

Tumor cell lines

The A549 (DSMZ Cat# ACC-107, RRID:CVCL_0023) and MDA-MB-231 (ATCC Cat# HTB-26, RRID:CVCL_0062) cell lines were purchased from DSMZ (Leibnitz-Institut Deutsche Sammlung von Mikroorganismen und Zellkulturen) and ATCC (American Type Culture Collection), respectively. Both cell lines were cultured in RPMI + 10 % FCS as directed.

ROR1-CAR and preparation of CAR T-cell lines

Lentiviral vectors encoding ROR1-CARs comprising an scFv derived from either the rabbit anti-human ROR1 mAb R12, or the mouse anti-human mAB 2A2, a short IgG4-Fc hinge or long IgG4-Fc hinge-C_H2-C_H3 spacer, a CD28 transmembrane domain, and a signaling module of 4-1BB_CD3ζ or CD28_CD3ζ have been described (5, 11). In each vector, the CAR transgene is separated by a T2A element from a truncated epidermal growth factor receptor (EGFRt) as transduction marker (41). $CD8^+$ and $CD4^+$ T-cells were purified by immunomagnetic separation (Miltenyi) and activated with anti-CD3/CD28 beads (Thermo Fisher), prior to lentiviral transduction, enrichment and expansion of CAR^+ (i.e. $EGFRt^+$) T-cells (42).

SISmuc scaffold and preparation of lung and breast cancer models

The SISmuc scaffold of porcine small intestine submucosa (SIS) and mucosa (muc), and the preparation of 3D tissues under static and dynamic conditions was performed according to established, standardized protocols (12–14, 43). In brief, jejunum was explanted, chemically decellularized with sodium desoxycholate monohydrate, and the mesentery and vascular tree removed. After γ-sterilization, the SISmuc was then fixed in a cell crown between two metal rings and $1x10^5$ A549 or MDA-MB-231 cells were seeded on the luminal side of the scaffold (Supplemental Figure 1A). The cell crowns were placed in 12-well plates with 2.5 ml RPMI-1640 + 10 % FCS medium, and complete medium changes performed every 2-3 days. After 11 days of culture, ROR1-CAR-modified or control T-cells were administered directly into the medium. For ELISA analyses, medium was obtained from the cell crown. Prior to dynamic culture, tumor cells were let to attach to the SISmuc for 3 days under static conditions and the scaffold then placed into the cassette of a customized tubing system in a bioreactor (Supplemental Figure 1B) (21, 44). The tubing system contained 45 ml of medium and a roller-pump continuously applied a constant medium flow with a velocity of 3-4 mL/min. After 14 days of dynamic culture, ROR1-CAR-modified or control T-cells were administered into a medium reservoir that was connected to the scaffold through an arterial and venous tube. For ELISA analyses, medium was aspirated through a sampling port.

ELISA for quantification of M30, IL-2 and IFN-γ

ELISA were performed according to the manufacturers' instructions (M30 Cytodeath ELISA, Peviva; IL-2 and IFN-γ, BioLegend). All samples were analyzed as technical duplicates.

Re-isolation of tumor cells

Tumor cells were re-isolated from the SISmuc scaffold for subsequent flow cytometric analyses. The scaffolds were washed with PBS/EDTA, Trypsin/EDTA applied for approx. 3 min and then, the reaction stopped with FCS. Cells were mobilized with a cell scraper, passed through a 40 µm cell sieve, pelleted by centrifugation for 5 min at 300 xg and resuspended in flow buffer.

Phenotypic analysis by flow cytometry

Fluorochrome-conjugated mAbs against CD4 (Miltenyi Biotec Cat# 130-113-258, RRID:AB_2726059), CD8 (Miltenyi Biotec Cat# 130-113-157, RRID:AB_2725985), CD279 (PD-1, Miltenyi Biotec Cat# 130-117-384, RRID:AB_2727929) and ROR1 (Miltenyi Biotec Cat# 130-098-317, RRID:AB_2653359) all from Miltenyi, CD8a (BioLegend Cat# 301006, RRID:AB_314124), CD69 (BioLegend Cat# 310906, RRID:AB_314841) and CD274 (PD-L1, BioLegend Cat# 329708, RRID:AB_940360) from Biolegend and CD25 (BD Biosciences Cat# 561399, RRID:AB_10643029) from BD were used according to the manufacturer's instructions. The anti-EGFR mAB Cetuximab (Bristol-Myers Squibb) was labelled in-house with Alexa-647 following the manufacturer's instructions (ThermoFisher). 7-AAD (BD) was used to exclude dead cells from analysis. A FACSCanto II (BD) was used for data acquisition and data analyses were performed using FlowJo v10.0.7 software (Tree Star).

Immunofluorescence staining

Scaffolds were fixed in 4 % paraformaldehyde (PFA), embedded in paraffin, and 3 µm cross-sections prepared using a microtome (Leica Microsystems). Immunofluorescence staining was performed with primary antibodies against collagen IV (Abcam Cat# ab6586, RRID:AB_305584), vimentin (Abcam Cat# ab92547, RRID:AB_10562134), Ki67 (Abcam Cat# ab16667, RRID:AB_302459) from Abcam, CD45 (Dako Cat# M0701, RRID:AB_2314143) from Agilent Dako, and pan-cytokeratin (Sigma-Aldrich Cat# C2562, RRID:AB_476839) from Sigma-Aldrich. All primary antibodies were diluted 1:100 and incubated overnight at 4 °C. Secondary antibodies specific for mouse IgG (Thermo Fisher Scientific Cat# A-31571, RRID:AB_162542) conjugated to Alexa-647 or specific for rabbit IgG (Thermo Fisher Scientific Cat# A-31572, RRID:AB_162543) conjugated to Alexa-555 were diluted 1:400 and incubated for 1 h at room temperature. Nuclei were counterstained by DAPI (Southern-

Biotech). Images were acquired using a digital microscope (BZ-9000, Keyence) or a confocal laser scanning microscope (SP-8, Leica Microsystems) and stored electronically in tiff format. Images were processed using the open-source software Fiji. All images were processed using the identical algorithm.

Analysis of T-cell proliferation by Ki67 staining

Immunofluorescence staining for CD45 and Ki67 was performed. Six (dynamic conditions) or ten (static) images per sample in 20x magnification were analyzed and the percentage of proliferating T-cells determined by dividing the number of $CD45^+Ki67^+$ by the number of $CD45^+$ cells.

Statistics

The open-source software R (CRAN, The Comprehensive R Archive Network) and GraphPad Prism 6.07 software (GraphPad Software) were used for statistical analyses. All experiments were independently repeated n=4 times unless stated otherwise. No samples were excluded from analysis. Two-tailed Student's t-test or Wilcoxon rank sum test were used with a confidence interval of 95 %, and results with a p value of < 0.05 were considered statistically significant.

Study approval

Peripheral blood was obtained from healthy donors after written informed consent to participate in research protocols approved by the Institutional Review Board of the University of Würzburg (Ethik-Kommission der Universität Würzburg, Würzburg, Germany).

The SISmuc scaffold was prepared from porcine intestine. All animals (local supplier) received humane care in compliance with the guidelines by the FELASA, WHO and FDA (WHO-TRS978 Annex3 und FDA-OCTGT Preclinical Guidance) after approval from the Institutional Animal Care and Use Committee of the University of Würzburg and the local competent authority (registration reference number #2532-2-12, Regierung von Unterfranken, Würzburg, Germany).

Authors' contributions

Conception and design: S.L. Nietzer, G. Dandekar, H. Walles, M. Hudecek.

Development of methodology: S.L. Nietzer, T. Schwarz, G. Dandekar, H. Walles, M. Hudecek

Acquisition of data (provided animals, acquired and managed patients, provided facilities, etc.): C. Göttlich, L.C. Nelke, L. Wallstabe, J. Kühnemundt

Analysis and interpretation of data (e.g., statistical analysis, biostatistics, computational analysis): C. Göttlich, L.C. Nelke, L. Wallstabe, J. Kühnemundt, T. Nerreter, G. Dandekar, S.L. Nietzer, M. Hudecek

Writing, review, and/or revision of the manuscript: C. Göttlich, L.C. Nelke, L. Wallstabe, J. Kühnemundt, T. Nerreter, H. Walles, H. Einsele, G. Dandekar, S.L. Nietzer, M. Hudecek

Administrative, technical, or material support (i.e., reporting or organizing data, constructing databases): T. Schwarz

Study supervision: S.L. Nietzer, G. Dandekar, H. Walles, H. Einsele, M. Hudecek

Acknowledgments

This research was supported by German Cancer Aid (Max Eder Program Award, Grant No. 70110313 to M.H.), by IZKF Würzburg (Interdisziplinäres Zentrum für Klinische Forschung; Projects Z4/109 & D-244 to M.H., and Project B-354 to M.H & G.D.) and the BayernFIT Program of the Bavarian state government (to H.W. & G.D.). M.H. is a member of the Young Scholar Program (Junges Kolleg) and Extraordinary Member of the Bavarian Academy of Sciences (Bayerische Akademie der Wissenschaften).

References

1. Turtle CJ et al. CD19 CAR-T cells of defined CD4+:CD8+ composition in adult B cell ALL patients. *J. Clin. Invest.* 2016;126(6):2123–38.

2. Neelapu SS et al. Axicabtagene Ciloleucel CAR T-Cell Therapy in Refractory Large B-Cell Lymphoma. *N. Engl. J. Med.* 2017;377(26):2531–2544.

3. Maude SL et al. Tisagenlecleucel in Children and Young Adults with B-Cell Lymphoblastic Leukemia. *N. Engl. J. Med.* 2018;378(5):439–448.

4. Hudecek M et al. The B-cell tumor-associated antigen ROR1 can be targeted with T cells modified to express a ROR1-specific chimeric antigen receptor. *Blood* 2010;116(22):4532–41.

5. Hudecek M et al. Receptor affinity and extracellular domain modifications affect tumor recognition by ROR1-specific chimeric antigen receptor T cells. *Clin. Cancer Res.* 2013;19(12):3153–64.

6. Baskar S et al. Unique cell surface expression of receptor tyrosine kinase ROR1 in human B-cell chronic lymphocytic leukemia. *Clin. Cancer Res.* 2008;14(2):396–404.

7. Zhang S et al. The onco-embryonic antigen ROR1 is expressed by a variety of human cancers. *Am. J. Pathol.* 2012;181(6):1903–10.

8. Balakrishnan A et al. Analysis of ROR1 Protein Expression in Human Cancer and Normal Tissues. *Clin. Cancer Res.* 2017;23(12):3061–3071.

9. Berger C et al. Safety of targeting ROR1 in primates with chimeric antigen receptor-modified T cells. *Cancer Immunol. Res.* 2015;3(2):206–16.

10. Yamaguchi T et al. NKX2-1/TITF1/TTF-1-Induced ROR1 is required to sustain EGFR survival signaling in lung adenocarcinoma. *Cancer Cell* 2012;21(3):348–61.

11. Hudecek M et al. The nonsignaling extracellular spacer domain of chimeric antigen receptors is decisive for in vivo antitumor activity. *Cancer Immunol. Res.* 2015;3(2):125–35.

12. Linke K, Schanz J, Hansmann J, Walles T, Brunner H, Mertsching H. Engineered liver-like tissue on a capillarized matrix for applied research. *Tissue Eng.* 2007;13(11):2699–707.

13. Stratmann AT et al. Establishment of a human 3D lung cancer model based on a biological tissue matrix combined with a Boolean in silico model. *Mol. Oncol.* 2014;8(2):351–65.

14. Göttlich C et al. A Combined 3D Tissue Engineered In Vitro/In Silico Lung Tumor Model for Predicting Drug Effectiveness in Specific Mutational Backgrounds. *J. Vis. Exp.* 2016;(110):e53885.

15. Göttlich C et al. A combined tissue-engineered/in silico signature tool patient stratification in lung cancer. *Mol. Oncol.* 2018;12(8):1264–1285.

16. Sommermeyer D et al. Chimeric antigen receptor-modified T cells derived from defined CD8+ and

CD4+ subsets confer superior antitumor reactivity in vivo. *Leukemia* 2016;30(2):492–500.

17. Newick K, O'Brien S, Moon E, Albelda SM. CAR T Cell Therapy for Solid Tumors. *Annu. Rev. Med.* 2017;68(1):139–152.

18. Wegner A. Chimeric antigen receptor T cells for the treatment of cancer and the future of preclinical models for predicting their toxicities *Immunotherapy* 2017;9(8):669–680.

19. Paszek MJ et al. Tensional homeostasis and the malignant phenotype. *Cancer Cell* 2005;8(3):241–54.

20. Walles T, Weimer M, Linke K, Michaelis J, Mertsching H. The potential of bioartificial tissues in oncology research and treatment. *Onkologie* 2007;30(7):388–94.

21. Nietzer S et al. Mimicking Metastases Including Tumor Stroma: A New Technique to Generate a Three-Dimensional Colorectal Cancer Model Based on a Biological Decellularized Intestinal Scaffold. *Tissue Eng. Part C. Methods* 2016;22(7):621–35.

22. Kenny PA et al. The morphologies of breast cancer cell lines in three-dimensional assays correlate with their profiles of gene expression. *Mol. Oncol.* 2007;1(1):84–96.

23. Carterson AJ et al. A549 lung epithelial cells grown as three-dimensional aggregates: alternative tissue culture model for Pseudomonas aeruginosa pathogenesis. *Infect. Immun.* 2005;73(2):1129–40.

24. McLachlan E, Shao Q, Wang H-L, Langlois S, Laird DW. Connexins act as tumor suppressors in three-dimensional mammary cell organoids by regulating differentiation and angiogenesis. *Cancer Res.* 2006;66(20):9886–94.

25. Pavesi A et al. A 3D microfluidic model for preclinical evaluation of TCR-engineered T cells against solid tumors. *JCI insight* 2017;2(12):e89762.

26. Valignat M-P, Theodoly O, Gucciardi A, Hogg N, Lellouch AC. T lymphocytes orient against the direction of fluid flow during LFA-1-mediated migration. *Biophys. J.* 2013;104(2):322–31.

27. John LB et al. Anti-PD-1 antibody therapy potently enhances the eradication of established tumors by gene-modified T cells. *Clin. Cancer Res.* 2013;19(20):5636–46.

28. Barber DL et al. Restoring function in exhausted CD8 T cells during chronic viral infection. *Nature* 2006;439(7077):682–7.

29. Rupp LJ et al. CRISPR/Cas9-mediated PD-1 disruption enhances anti-tumor efficacy of human chimeric antigen receptor T cells. *Sci. Rep.* 2017;7(1):737.

30. Wallstabe L, Mades A, Frenz S, Einsele H, Rader C, Hudecek M. CAR T cells targeting αvβ3 integrin are effective against advanced cancer in preclinical models. *Adv. cell gene Ther.* 2018;1(2):e11.

31. Yang J, Baskar S, Kwong KY, Kennedy MG, Wiestner A, Rader C. Therapeutic potential and challenges of targeting receptor tyrosine kinase ROR1 with monoclonal antibodies in B-cell malignancies. *PLoS One* 2011;6(6):e21018.

32. Baskar S, Wiestner A, Wilson WH, Pastan I, Rader C. Targeting malignant B cells with an immunotoxin against ROR1. *MAbs* 2012;4(3):349–61.

33. Lübtow MM et al. Drug induced micellization into ultra-high capacity and stable curcumin nanoformulations: Physico-chemical characterization and evaluation in 2D and 3D in vitro models. *J. Control. Release* 2019;303:162–180.

34. Mertsching H et al. Generation and transplantation of an autologous vascularized bioartificial human tissue. *Transplantation* 2009;88(2):203–10.

35. Hoppensack A et al. A human in vitro model that mimics the renal proximal tubule. *Tissue Eng. Part C. Methods* 2014;20(7):599–609.

36. Steinke M, Dally I, Friedel G, Walles H, Walles T. Host-integration of a tissue-engineered airway patch: two-year follow-up in a single patient. *Tissue Eng. Part A* 2015;21(3–4):573–9.

37. Groeber F et al. A first vascularized skin equivalent as an alternative to animal experimentation. *ALTEX* 2016;33(4):415–422.

38. Schweinlin M et al. Development of an Advanced Primary Human In Vitro Model of the Small Intestine. *Tissue Eng. Part C. Methods* 2016;22(9):873–83.

39. Weigel T et al. A three-dimensional hybrid pacemaker electrode seamlessly integrates into engineered, functional human cardiac tissue in vitro. *Sci. Rep.* 2018;8(1):14545.

40. Colunga T et al. Human Pluripotent Stem Cell-Derived Multipotent Vascular Progenitors of the Mesothelium Lineage Have Utility in Tissue Engineering and Repair. *Cell Rep.* 2019;26(10):2566-2579.e10.

41. Wang X et al. A transgene-encoded cell surface polypeptide for selection, in vivo tracking, and ablation of engineered cells. *Blood* 2011;118(5):1255–63.

42. Riddell SR, Greenberg PD. The use of anti-CD3 and anti-CD28 monoclonal antibodies to clone and expand human antigen-specific T cells. *J. Immunol. Methods* 1990;128(2):189–201.

43. Schanz J, Pusch J, Hansmann J, Walles H. Vascularised human tissue models: a new approach for the refinement of biomedical research. *J. Biotechnol.* 2010;148(1):56–63.

44. Schuerlein S et al. A versatile modular bioreactor platform for Tissue Engineering. *Biotechnol. J.* 2017;12(2):1600326.

Figures and Figure legends

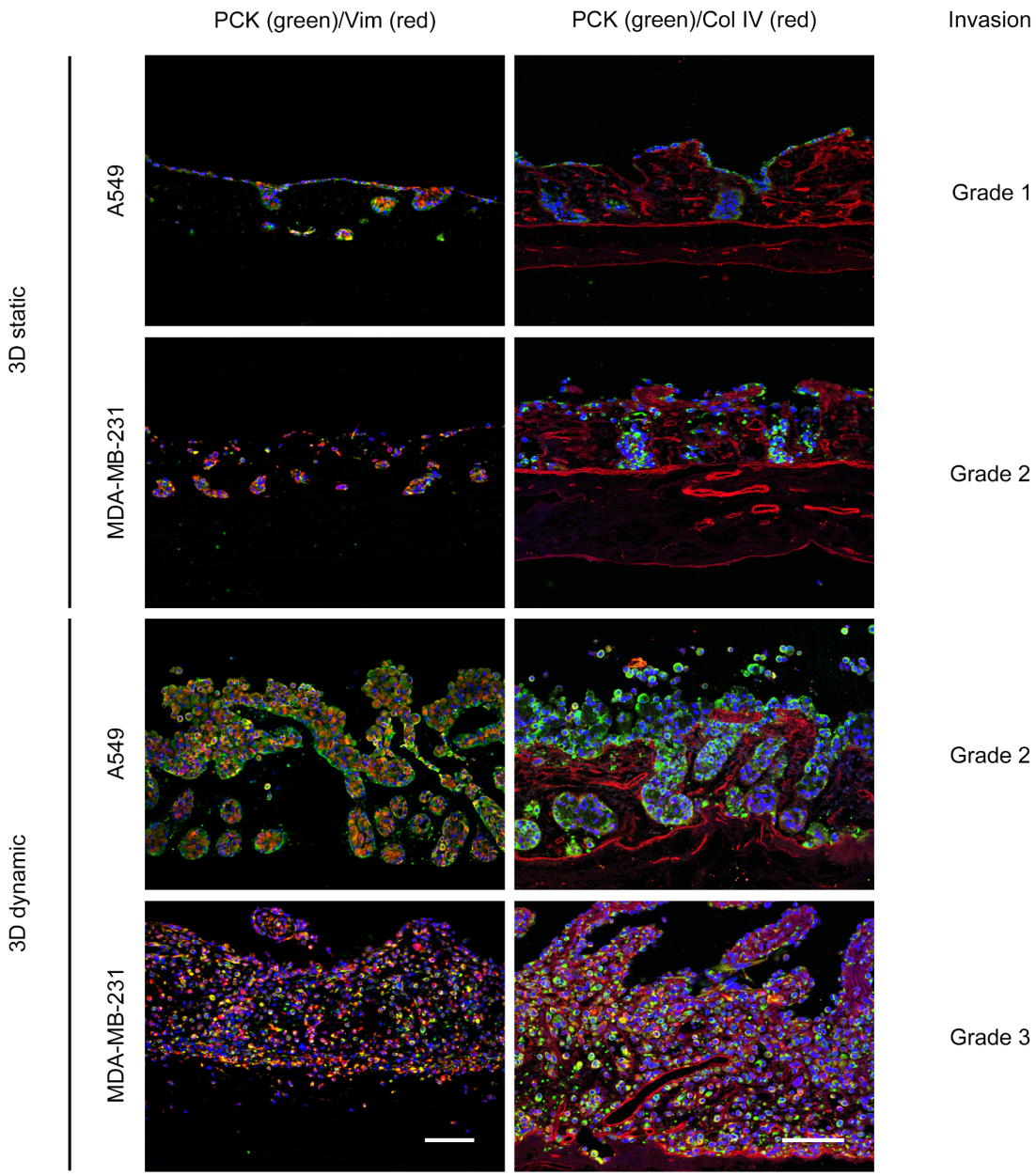

Figure 1. Invasive growth of A549 lung cancer and MDA-MB-231 breast cancer in 3D culture. The tumor cell lines A549 (lung cancer) and MDA-MB-231 (breast cancer) were cultured on SISmuc scaffold under static (upper panel) and dynamic (lower panel) culture conditions, resp., and tumor composition and architecture were evaluated by immunofluorescence staining. Left column: pan-cytokeratin (PCK, green) and vimentin (Vim, red). Nuclei are counterstained with DAPI (blue). Right column: PCK (green) and collagen IV (Col IV, red). Nuclei are counterstained with DAPI (blue). 100 µm scale bars in lower images are representative for all images of a column. Grading was performed according to scheme presented in Table 1.

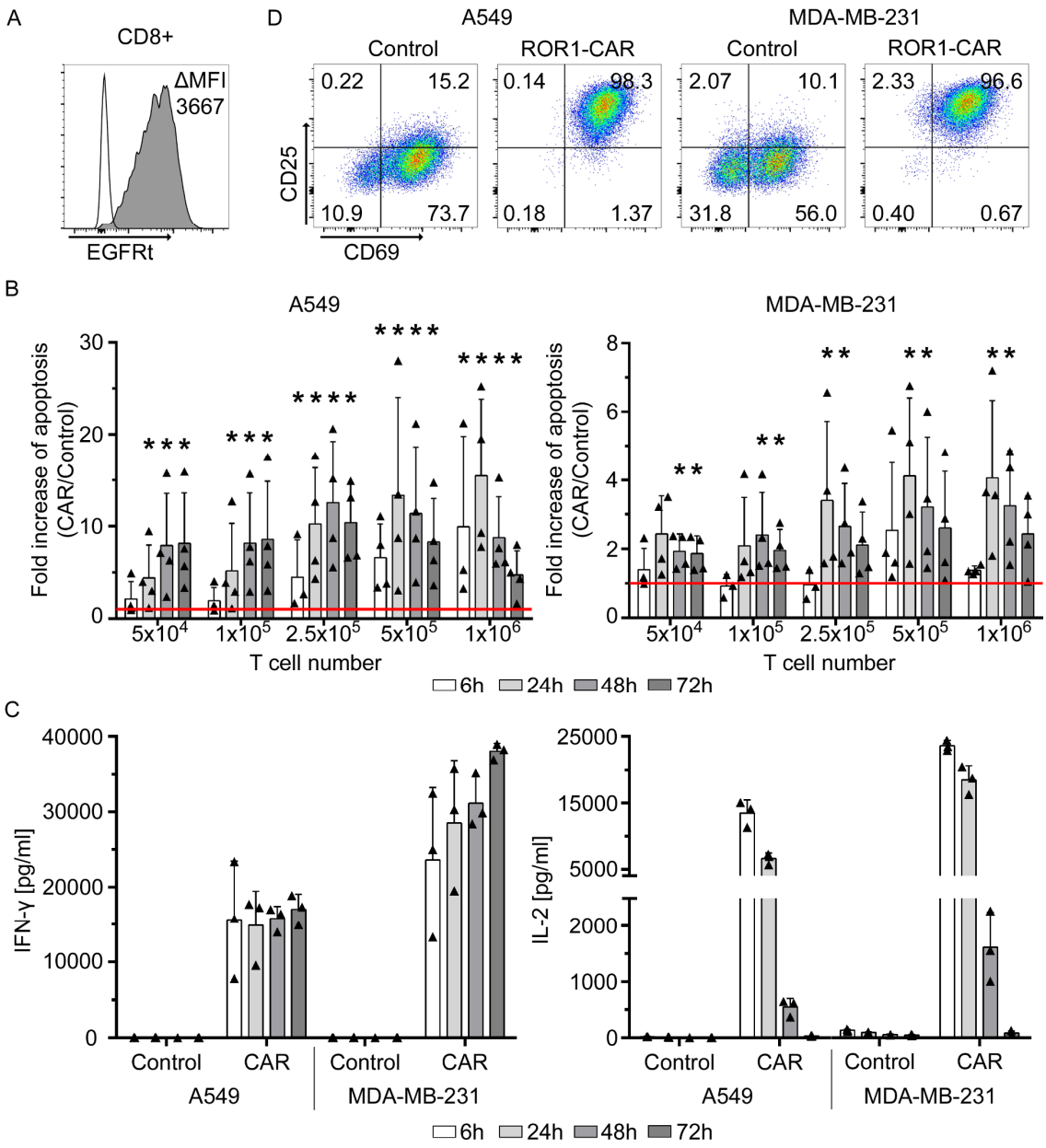

Figure 2. ROR1-CAR T-cells induce apoptosis of 3D lung cancer and breast cancer in static culture. A, Expression of EGFRt transduction marker on CD8$^+$ ROR1-CAR T-cells prior to functional testing. ΔMFI depicts the difference in geometric mean fluorescence intensity between ROR1-CAR T-cells and unmodified control T-cells. **B**, Quantification of apoptosis induced by ROR1-CAR T-cell treatment with increasing CD8$^+$ T-cell numbers for 72 h. Apoptosis was measured with M30-ELISA from supernatants collected at the indicated time point and is presented as x-fold change compared to the respective control T-cell treatment (red line). n=4, data are presented as arithmetic mean + SD, Wilcoxon rank sum test: * $p < 0.05$. **C**, ELISA-based quantification of IFN-γ and IL-2 from supernatants collected at the indicated time point from static tumor models treated with 1x10^6 T-cells for 72 h. Data are presented as arithmetic mean of three cell crowns from n=1 experiment + SD. **D**, Expression of CD25 and CD69 on CD8$^+$ ROR1-CAR T-cells and unmodified control T-cells at the end of the 72 h analysis period in the static tumor model. One representative plot of n=3 experiments is shown.

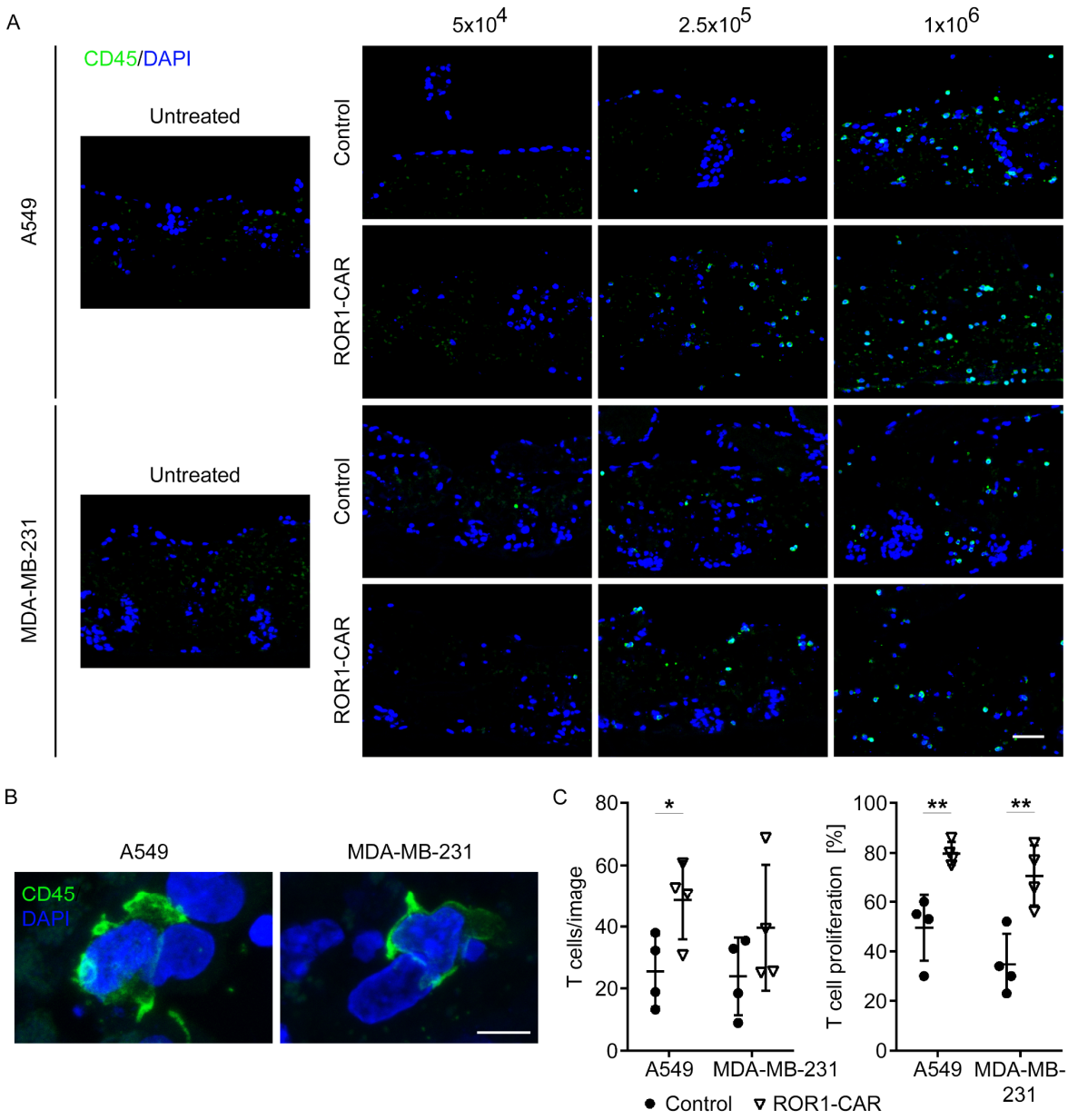

Figure 3. ROR1-CAR T-cells migrate into tumor tissue and proliferate in static 3D culture. A, Immunofluorescence staining of lymphocyte marker CD45 (green) on paraffin sections of untreated tumor models (untreated) or tumor models treated with increasing concentrations ($5x10^4$, $2.5x10^5$, $1x10^6$) of unmodified $CD8^+$ control T-cells (Control) or $CD8^+$ ROR1-CAR T-cells (ROR1-CAR). Nuclei are counterstained with DAPI. Scale bar: 50 µm. **B**, Close-up of CD45 immunofluorescence staining (green) on paraffin sections of $CD8^+$ ROR1-CAR T-cell treated 3D tumor models. Nuclei are counterstained with DAPI (blue). Scale bar: 10 µm. **C**, Mean number of T-cells per image and proliferation of T-cells in static 3D tumor models treated with $5x10^4$ unmodified $CD8^+$ control T-cells (Control) or $CD8^+$ ROR1-CAR T-cells (ROR1-CAR) assessed by quantification of Ki67/CD45 immunofluorescence double-staining. $CD45^+$ and $Ki67/CD45^+$ cells were counted in ten images per condition. n=4, data are presented as arithmetic mean + SD, student's t-test: * $p < 0.05$, ** $p < 0.01$.

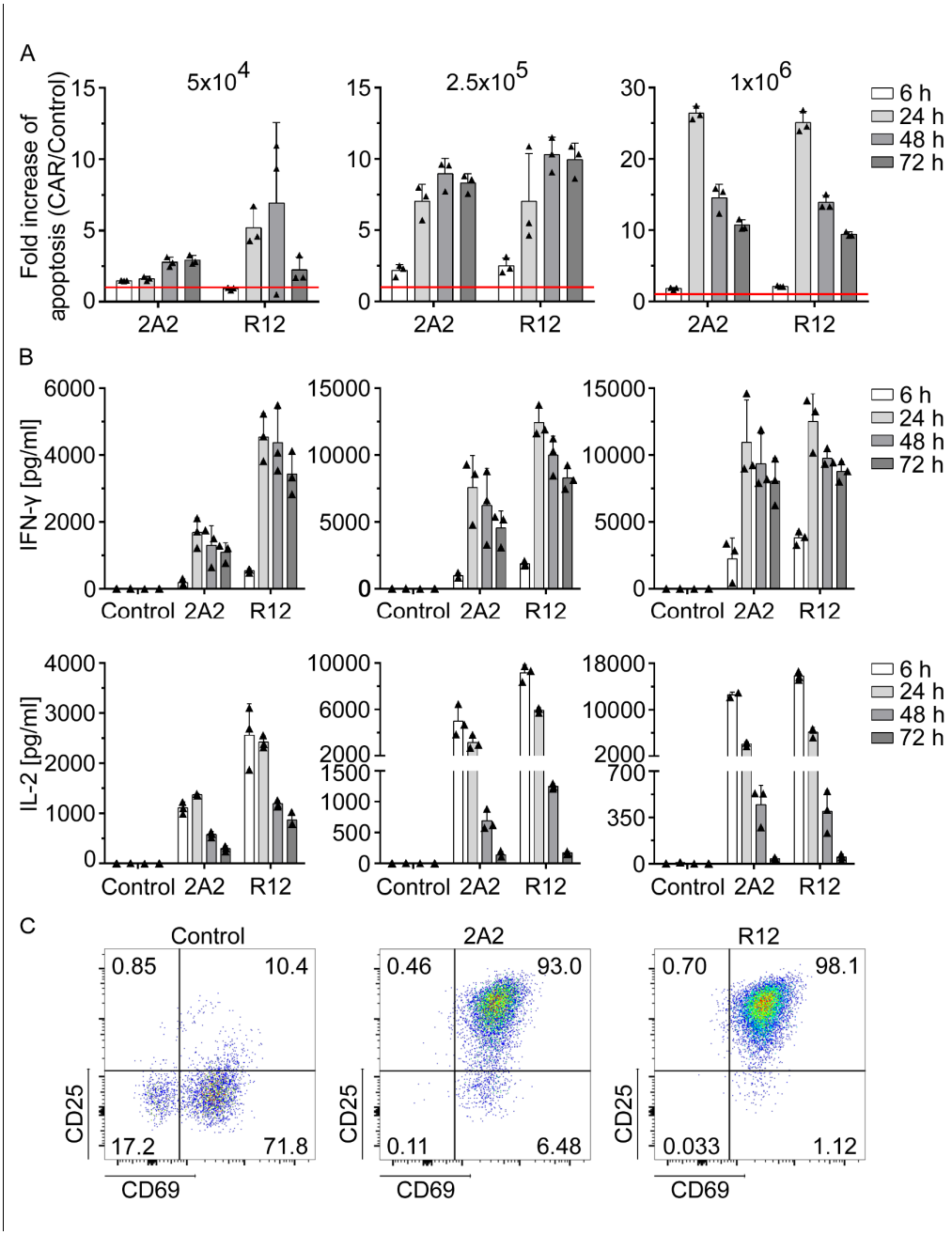

Figure 4. Variations in ROR1-CAR targeting domain affect anti-tumor function in 3D lung cancer models. A, Quantification of apoptosis induced by ROR1-CAR T-cells with either 2A2 or R12 targeting domains during 72 h treatment with increasing $CD8^+$ T-cell dose ($5x10^4$, $2.5x10^5$, $1x10^6$). Apoptosis was measured with M30-ELISA from supernatants collected at the indicated time point and is presented as x-fold change compared with the same dose of control T-cells (red line). Data are presented as arithmetic mean of three cell crowns from n=1 experiment + SD. **B**, ELISA-based quantification of IFN-γ and IL-2 from supernatants collected at the indicated time point from static tumor models treated with increasing $CD8^+$ T-cell numbers for 72 h. Data are presented as arithmetic mean of three cell crowns from n=1 experiment + SD. **C**, Expression of CD25 and CD69 on $CD8^+$ ROR1-CAR T-cells and unmodified control T-cells at the end of the 72 h analysis period in the static tumor model. One representative plot of three cell crowns from n=1 experiment is shown.

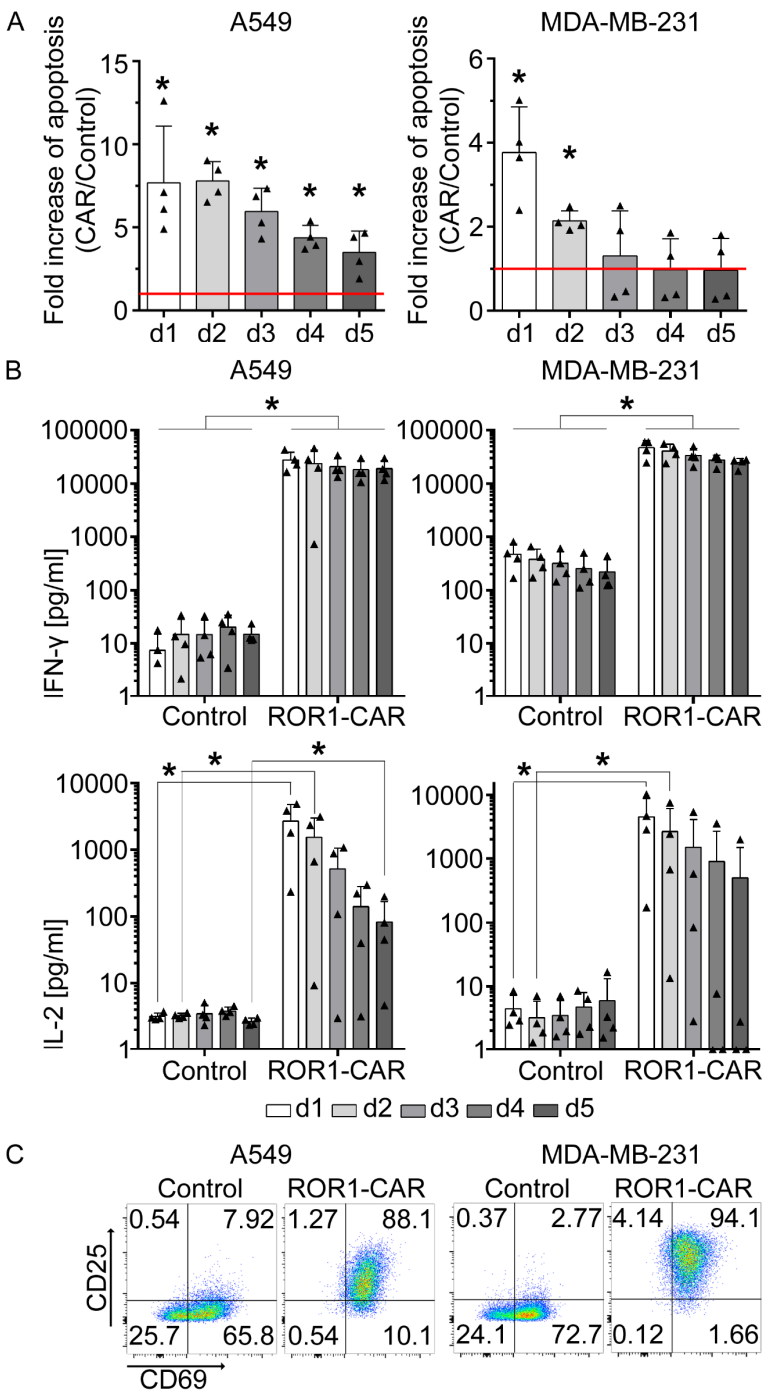

Figure 5. ROR1-CAR T-cells induce tumor cell apoptosis of 3D lung and breast cancer in dynamic culture. A, Quantification of apoptosis induced by ROR1-CAR T-cells during five days of treatment. Apoptosis was measured with M30-ELISA from supernatants collected at the indicated time point and is presented as x-fold change compared to the respective control T-cell treatment (red line). n=4, data are presented as arithmetic mean + SD, Wilcoxon rank sum test: * $p < 0.05$. **B**, ELISA-based quantification of IFN-γ and IL-2 from supernatants collected over time from dynamic tumor models treated with T-cells for five days. n=4, data are presented as arithmetic mean + SD, Wilcoxon rank sum test: * $p < 0.05$. **C**, After five days of treatment, $CD8^+$ T-cells were analyzed for expression of CD25 and CD69 by flow cytometry. One representative plot of n=4 experiments is shown.

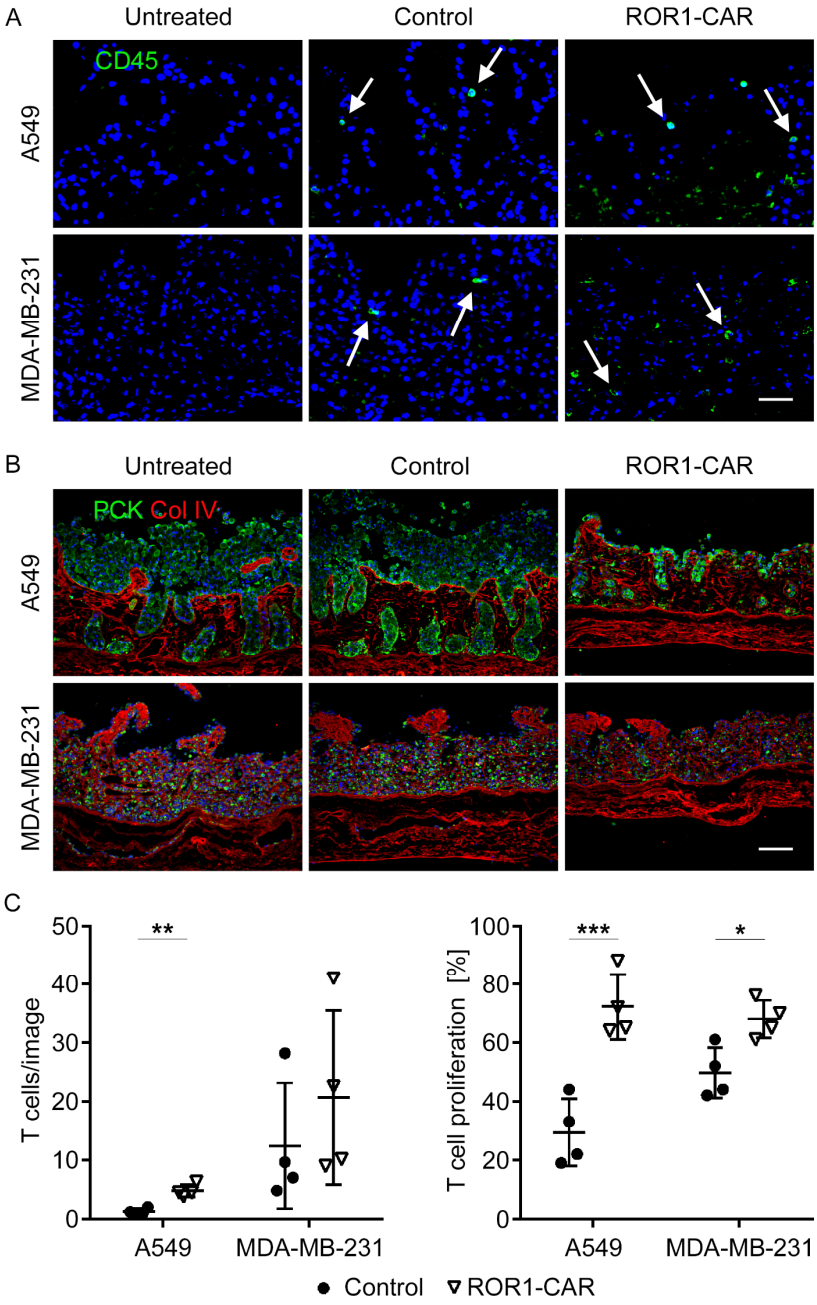

Figure 6. ROR1-CAR T-cell migrate into tumor tissue and induce tumor cell lysis in a dynamic 3D culture. A, Immunofluorescence staining of CD45 (green) on paraffin sections of dynamic tumor models treated with control or ROR-1 CAR T-cells. White arrows mark T-cells that had migrated into the tissue matrix. Nuclei are counterstained with DAPI (blue). Scale bar: 100 µm. **B**, Immunofluorescence double-staining of PCK (green) and Col IV (red) on paraffin sections of untreated dynamic tumor models as well as tumor models treated with $CD4^+$ and $CD8^+$ untransduced control T-cells or $CD4^+$ and $CD8^+$ ROR1-CAR T-cells with a total T-cell number of $1x10^7$ per condition. Scale bar: 100 µm. **C**, Mean number of T-cells per image and T-cell proliferation assessed by quantification of Ki67/CD45 immunofluorescence double-staining. $CD45^+$ and $Ki67/CD45^+$ cells were counted in ten images per condition. n=4, data are presented as arithmetic mean + SD, Student's t-test: * $p < 0.05$, ** $p < 0.01$, *** $p < 0.001$.

Tables

Table 1. Grades of invasiveness represented by the 3D tumor models

Grade	Phenotype	Represented by model
1	Tumor cells populate former crypt structures, but do not cross the basement membrane	A549 / static culture
2	Single tumor cells cross the basement membrane, crypt structure is preserved	MDA-MB-231 / static culture A549 / dynamic culture
3	Tumor cells cross the basement membrane and infiltrate the extracellular matrix (ECM), thereby disrupting crypt structure morphology	MDA-MB-231 / dynamic culture